CHEMISTRY
A European Journal

A Journal of
ChemPubSoc Europe

Accepted Article

Title: Solvent-tuned supramolecular assembly of fluorescent catechol/ pyrene amphiphilic molecules

Authors: Fabiana Nador, Karolina Wnuk, Claudio Roscini, Ruben Solorzano, Jordi Faraudo, Daniel Ruiz-Molina, and Fernando Novio

To be cited as: *Chem. Eur. J.* 10.1002/chem.201802249

Link to VoR: http://dx.doi.org/10.1002/chem.201802249

Supported by
ACES

WILEY-VCH

10.1002/chem.201802249

WILEY-VCH

Solvent-tuned supramolecular assembly of fluorescent catechol/pyrene amphiphilic molecules

F. Nador,[a,b]* K. Wnuk,[a] C. Roscini,[a] R. Solorzano,[a,c] J. Faraudo,[d] D. Ruiz-Molina[a] and F. Novio[a,c]*

Abstract: The synthesis and structuration of a novel low molecular amphiphilic catechol **1** is reported. The combination of a hydrophilic tail containing a catechol group and a pyrene-based hydrophobic head favors its solvent tuned supramolecular assembly. Formation of hollow nanocapsules/vesicles occurs in concentrated solutions of both polar protic and non-protic organic solvents, whereas in water a fibril-like aggregation process is favored even at low concentrations. The emission properties of the pyrene moiety have allowed the monitoring of the self-assembly process which could be confirmed by optical and electronic microscopy. In organic solvents and at low concentrations, compound **1** remains on its non-assembled monomeric form. As the concentration increases, the aggregation containing pre-associated pyrene moieties becomes more evident up to a critical micellar concentration where vesicle-like structures are formed. In contrast, nanosized twist belt-like fibers have been observed in water even at low concentrations, meanwhile at high concentration microplate structures appears. The interactions between molecules in different solvents have been studied by molecular dynamics simulations, which have confirmed different solvent driven supramolecular interactions.

Introduction

Self-assembly involves the organization of atoms, molecules, particles and other building blocks into functional structures driven by different non-covalent bonds like hydrogen bonds, Van der Waals forces and hydrophobic or aromatic interactions.[1,2] Specifically, amphiphilic molecules such as surfactants, copolymers, and proteins, play a critical role in a wide range of self-assembly phenomena. Due to their dual nature, hydrophobic and hydrophilic part, they display a rich self-assembly behavior in solution. Depending on the molecule characteristics, structuration at the interface between immiscible media with different polarity will be induced. In this way different structures like micelles, fibers or vesicles can be obtained after the self-assembly process, founding interesting applications in biomimetics,[3] functional nanomaterials,[4] light harvesting[5] and drug and gene delivery.[6]

Specifically, the self-assembly processes of catechol-based molecules has attracted much interest and have been extensively studied due to their multiple roles and functions in nature and materials,[7] For instance, self-assembled monolayers (SAM) with enhanced adhesion properties mimicking those found for mussels have been reported by using the 4-(6′-mercaptohexyl)catechol on different gold surfaces.[8] Relevant information on the basic principles that govern the adhesion of catechols at the solid-liquid interface has also been obtained upon studying their self-assembly on different surfaces with scanning tunneling microscopy (STM).[9] The precise development and immobilization of functionalized self-assemble structures has provide also new (bio)active coatings with promising clinical or technological applications.[10] Moreover, the supramolecular self-assembly driven by catechol–metal ion coordination has afforded the fabrication of novel functional materials including adhesives, capsules, coatings and hydrogels,[11] as well the formation of coordination polymer nanoparticles of technological relevance in different areas such as molecular electronics or nanomedicine.[12] The formation of coordination bonds with specific metals can improve the mechanical properties and control of the self-assembly process catechol-metal coordination.

The supramolecular assembly of catechol-containing amphiphilic copolymers or peptides as micelles or vesicles has also been a theme of interest. Hasewaga *et al.* have reported micelles made from poly(ethylene glycol)-b-poly(dopamine) block copolymers with antioxidant and scavenging activity in front of reactive oxygen species (ROS).[13] Dai *et al.* have reported a supramolecular approach combining both catechol-metal ion coordination and polymer self-assembly that organizes polymers from solid particles or homogeneous vesicles to Janus vesicles.[11a] In the same way, Pierre *et al*. have reported the self-assembly properties of three synthetic amphiphilic chelators consisting of monopodal or tripodal catechol ligands bearing long alkyl chains.[14]

On the other hand, it is well known that pyrene moieties are able to self-aggregate establishing weak intermolecular interactions (i.e. π-π interactions) to form ordered mesophases.[15] or even induce supramolecular chirality.[16] Moreover, pyrene optical properties (absorption and luminescence) are highly sensitive to the medium polarity and to

[a] Dr. F. Nador, K. Wnuk, Dr. C. Roscini, R. Solorzano, Dr. D. Ruiz-Molina, Dr. F. Novio
Catalan Institute of Nanoscience and Nanotechnology (ICN2), CSIC and The Barcelona Institute of Science and Technology, Edificio ICN2, Campus UAB, Bellaterra, 08193 Barcelona, Spain.
E-mail: fabiana.nador@uns.edu.ar; fernando.novio@icn2.cat
[b] Dr. F. Nador
Instituto de Química del Sur (INQUISUR-CONICET), Departamento de Química, Universidad Nacional del Sur, Av. Alem 1253, 8000 Bahía Blanca, Argentina.
[c] Dr. F. Novio, R. Solorzano
Departament de Química, Universitat Autònoma de Barcelona (UAB), Campus UAB. Cerdanyola del Vallès 08193, Barcelona, Spain
[d] Dr. J. Faraudo
Institut de Ciència de Materials de Barcelona (ICMAB-CSIC)
Campus UAB, E-08193 Bellaterra, Spain.

Supporting Information is available from the Wiley Online Library or from the author: experimental details, NMR, FT-IR, fluorescence and UV-Vis spectra, SEM and TEM microscopies and fluorescence images (PDF). 3D reconstruction video (avi).

the molecular packing processes and supramolecular associations in the microenvironment surrounding the probe, which makes it a good sensor for self-assembly processes and micelles/vesicles formation.[17,18]

This work is primarily aimed at controlling and tuning the supramolecular self-assembly process between catechol-containing amphiphilic molecules with two different moieties able to stablish intermolecular interactions. Herein we report the obtaining of hollow nanocapsules/vesicles formed from the self-direct assembly of the novel amphiphile molecule **1** (N-(3,4-dihydroxybenzylidene)-4-(pyren-1-yl)butanehydrazide), made of a hydrophilic catechol tail and a pyrene hydrophobic head (Scheme 1). Two main aspects have been studied: 1) the influence of concentration in self-assembly process, and 2) the molecular packing rearrangement as well as reversible morphological transformation influenced by the use of different solvents. The molecule was found *a)* to form hollow nanocapsules/vesicles in MeOH and acetone, *b)* nanosized twist belt-like fibers or microplates in water and *c)* presents reversible solvent-dependent self-assembly processes defined by the solvent nature and critical concentration (C_c). The self-aggregation behaviour was investigated by spectroscopic and microscopic techniques. Moreover, theoretical calculations were performed to study the balanced participation of hydrogen bonding and π-π stacking interactions.

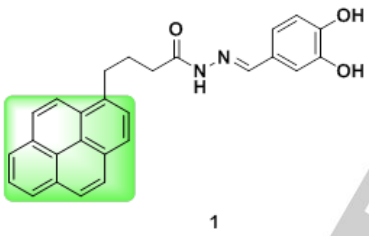

1

Scheme 1. Structure of compound **1** containing a pyrene hydrophobic part (in green) and the more hydrophilic catechol-based moiety.

Results and Discussion

Supramolecular assembly in MeOH

Compound **1** was synthesized by a coupling reaction between 4-(pyren-1-yl)butanehydrazide (PBH) and 3,4-dihydroxybenzaldehyde following the procedure described in Materials and Methods Section (see Supporting Information S1). The self-assembly process of **1** in methanol was initially followed by fluorescence and UV-Vis spectroscopies in the concentration range of 3.9 10^{-3} to 7.9 mM. The emission spectra (λ_{exc} = 340 nm) of low-concentrated MeOH solutions (3.9 10^{-3} mM) present the fine vibronic structure (λ_{max} = 376, 395 and 418 nm) typically obtained for substituted pyrene molecules in water (Figure 1a).[19] Upon increasing the concentration of **1**, different trends of the spectral features were observed, providing direct information on *a)* environmental changes around the amphiphilic molecule and *b)* the intermolecular interactions between pyrene moieties. Initially, the increase of the concentration of **1** (up to 7.9 10^{-2} mM) induced the expected progressive emission intensity enhancement (Figures 1a-b). Between 7.9 10^{-2} - 7.9 10^{-1} mM the emission intensity decreases significantly (Figure 1a-b), while no other bands appear. This quenching of fluorescence was associated to the intermolecular interactions between the molecules which start organizing in labile aggregates favored by the decrease of the spatial distance of pyrene moieties. Above 7.9 10^{-1} mM, the monomer emission keeps reducing its intensity for increased concentrations (Figure 1a). However, at these concentrations, the typical broad band emission corresponding to associated pyrene molecules (in the ground or excited electronic state) at 480 nm appears and increases with the molecule concentration, becoming the main contribution to the emission spectra as confirmed by the I_{480}/I_{376} values (Figure 1c). As commented, the unique spectral features of pyrene are highly sensitive to the microenvironment of the probe: it exhibits an ensemble of monomer fluorescence emission peaks that report on the polarity of the probe microenvironment, and an additional band at longer wavelengths which reflects the presence of another pyrene molecule in spatial proximity.[20] It is worth mentioning that any inner filter effect was excluded as the cause for the intensity decrease since a triangular cuvette and front-face setup were used to measure the concentration dependent spectra and no deformations of the spectra (due to the partial emission reabsorption) were observed.[21]

In order to obtain further information on the system from the obtained spectra, we determined the R_I factor, which provides hints on the polarity of the environment of pyrene molecules that can be caused by the proximity of other molecules of the same nature. It is, calculated as the ratio (I_I/I_{II})

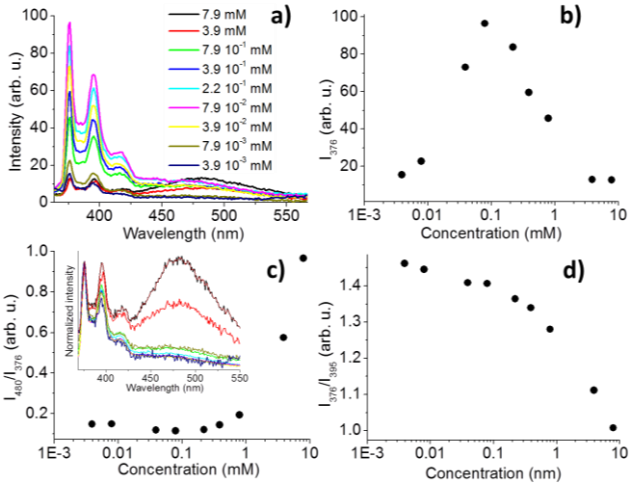

Figure 1. a) Emission spectra (λ_{exc} = 340 nm) of **1** in MeOH at different concentrations; b) Fluorescence intensity at 376 nm (I_{376}); c) RI (I_{376}/I_{395}) ratio and d) monomer/aggregate emission (I_{480}/I_{376}) ratio *vs* concentration (inset: normalized emission spectra).

between the band intensity of the emission spectra at λ_{max} = 376 nm (I_I), independent of the medium polarity, and the one at λ_{max} = 395 nm (I_{II}), which instead is dependent on the environment.[18] Therefore R_I is larger in polar solvents (e.g. R_I = 1.6 in water),

and decreases in hydrophobic media (e.g. R_I = 0.6 in alkanes).[18,22] In the present system, R_I stays above 1.4 (Figure 1d) until reaching the concentration at which is observed the highest emission intensity (7.9 10^{-2} mM) and decreases to 1.3 when the concentration becomes one order of magnitude higher (7.9 10^{-1} mM), confirming that the fluorescence quenching is related to the formation of labile aggregates which reduce the environment polarity around the pyrene moiety. According to previous studies, the pyrene molecules of these labile aggregates should be at very short distance (< 40 Å), but far enough to avoid the characteristic aggregates emission,[17] Above 7.9 10^{-1} mM, stable aggregates of **1** with emission at 480 nm are instead obtained.

In order to discriminate between the formation of ground state aggregates and excited state dimers (or excimers), absorption and fluorescence excitation spectroscopies were used. Basically, excimers are originated from the interaction between a molecule in its excited state and another in the ground state, while ground state aggregates are already formed without excitation.[17] Though sometimes they show similar emission spectra (broad emission band with λ_{max} ~ 480 nm), the excitation and absorption spectra are useful tools to discriminate between these situations: since in excimers the initial excitation always involves the monomeric species, both excitation and absorption spectra shows the same band features of the monomer. On the other hand, because the aggregates are different species, the relative spectra should change respect to the monomer one.

Unfortunately, with absorption spectroscopy was only possible to measure some of the more diluted solutions of **1**, since at 7.9 10^{-1} mM saturation of the signal was observed even using a thinner 2 mm cuvette (see Supporting Information, Figure S6a). The parameter P_A, calculated as peak-to-valley ratio of the (0,0) vibronic transition (λ_{peak} = 343 nm and λ_{valley} = 333 nm) can be used as indicator of the association degree of the pyrene molecules, being values above 3 associated to the monomer and decreasing upon association. In the present case this value remains practically constant (~1.9) in the range of studied concentrations (see Supporting Information, Figure S6b), and only for the 7.9 10^{-1} mM solution the obtaining value was significantly below 2 (1.6). Since absorption measurements do not allow giving precise conclusions on the association degree, fluorescence measurements were performed at different concentrations. The excitation spectra of **1** obtained at λ_{emi} = 395 nm resemble, instead, that corresponding to the monomeric species (λ_{max} = 310, 323 and 339 nm)[18] until reaching the concentration of 7.9 10^{-2} mM (Figure 2a and Supporting Information, Figure S7). Above this concentration, the excitation spectra maintain a similar vibronic structure but shift to the red and reduce their intensity. Worth to mention is that the aggregation process is fully reversible, i.e. the monomeric fluorescence emission is completely recovered upon dilution.

The spectral data derived from excitation and emission spectra match with the macro- and microscopic appearance of the solutions. Up to 7.9 10^{-2} mM, when both maximum emission and monomeric spectral features are observed, completely transparent solutions were obtained (insets Figure 2) and no material structuration was observed by SEM (Figure 2b). The presence of labile aggregates by increasing the concentration and postulated from the fluorescence quenching is confirmed by the appearance of slightly cloudy solutions of **1** in MeOH and the inefficient formation of microstructured particles still mixed with non-structured materials (Figure 2c). Only when the concentration of **1** is in the range of the appearance of the aggregate emission in the visible region (λ_{emi} = 480 nm), the microparticles with mean size of 1.5 ± 0.5 μm, are efficiently and homogeneously formed as observed in SEM images yielding a very cloudy suspension (Figure 2d and 2e).

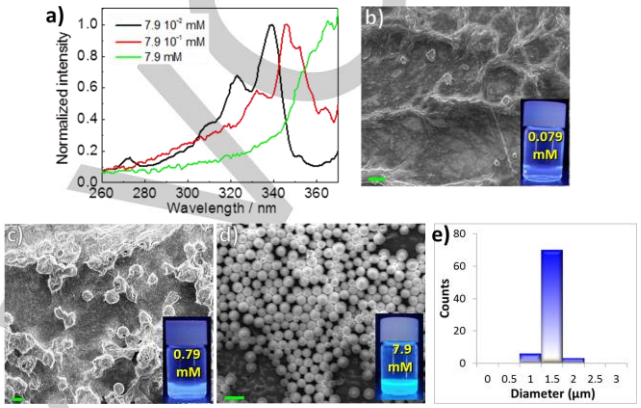

Figure 2. a) Normalized excitation spectra (λ_{emi} = 395 nm) of **1** at three different concentrations in MeOH; SEM images and digital photograph (insets) of solutions of **1** in MeOH at b) 7.9 10^{-2} mM, c) 7.9 10^{-1} mM and d) 7.9 mM. Scale bars are 2 μm. e) Histogram with size distribution for the particles at 7.9 mM.

Upon magnification of the images corresponding to high concentration solutions (7.9 mM), holes and fractured sections on a large fraction of the particles can be observed (see Supporting Information, Figure S8). According to previously reported works,[15a,23] the existence of these "open-mouth" structures is in agreement with the vesicle character of the structures and can be rationalized by the rigidity of the assembly, which would be responsible for the inability of the membranes to fully close. On the other hand, the formation of these relatively large hollow nanocapsules/vesicles is unknown at this stage, but it may arise from the fusion of smaller ones as the concentration of the molecules increases, as already described in the literature.[2,24] In fact, this was evidenced by STEM images, in which a detectable process of fusion between small particles resulted in the production of larger ones (see Supporting Information, Figure S9).

For corroborating that the formation of the hollow nanocapsules/vesicles is due to the amphiphilic character of the compound **1,** solutions containing different concentrations of PBH and 3,4-dihydroxybenzaldehyde were analized. No evidence of hollow nanocapsules/vesicles formation was obtained in the whole range of concentrations and only the presence of non-structured material was observed by SEM (see Supporting Information, Figure S10). These results confirm the need of having the pyrene and catechol units covalently linked forming the amphiphilic molecule **1** for a proper self-assembly.

The vesicle nature and the hollow features of this sample were also evidenced by fluorescence microscopy, where a clear contrast was observed between the walls and the inner areas of them (Figures 3a-b).[15c] At high concentrations (7.9 mM), the formation of hollow nanocapsules/vesicles with an emission around 470 nm after excitation at 405 nm was observed (Figure 3c).

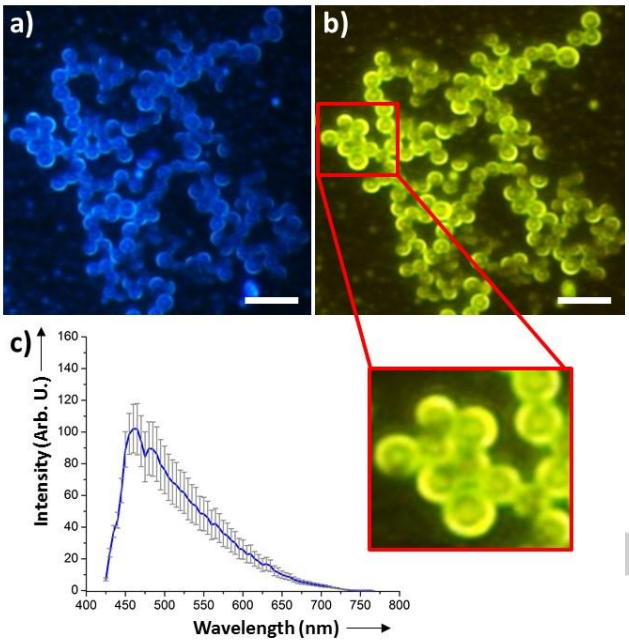

Figure 3. Fluorescence images for **1** in MeOH at 7.9 mM measured with a) DAPI (λ_{em} > 400 nm) and b) Alexa Fluor 488 (λ_{em} > 515 nm) filters. Scale bars are 5 μm. c) Average fluorescence spectrum with standard deviations after analysis on 10 representative hollow nanocapsules/vesicles (λ_{exc} = 405 nm).

Supramolecular assembly in acetone

The optical behavior of **1** was also studied in acetone in the same concentration range as that previously used for MeOH, exhibiting similar results (see Supporting Information, Figure S11). At low concentrations the emission spectrum is characteristic of the initial monomeric species (λ_{max} = 376, 396 nm and shoulder at 418 nm) with a fluorescence bands intensity enhancement along with a concentration increase, up to a value of 7.9 10^{-1} mM. A further increase of the concentration induced an inversion of the tendency, with a significant decrease of the bands between 350-450 nm and the appearing of a novel broad emission band at λ_{max}= 480 nm which increases up to the studied maximum concentration (7.9 mM). Similarly to what concluded for **1** in MeOH, this band is an indication of the pyrene molecules self-assembling in their ground state at higher concentrations, forming stable hollow nanocapsules/vesicles. The bathochromic shift and the loss of vibronic structure of the excitation spectra (λ_{emi} = 380 nm) also confirmed the formation of aggregates upon concentration of the compound in acetone (see Supporting Information, Figure S12). Also in this solvent, upon dilution the monomeric system can be reversibly obtained.

SEM images reveal again the formation of stable hollow nanocapsules/vesicles with average dimensions between 0.5 and 2.5 μm for concentrations above 3.9 mM. Below this value, some spherical structures were detected though quite polydispersed (see Supporting Information, Figure S13). Optical and fluorescence microscopy images of **1** in acetone at 7.9 mM showed the presence of a) large particles (between 2 and 4 μm) with holes on the surface and b) small particles (between 0.5 and 1 μm) with empty interior and fluorescent walls (see Supporting Information, Figure S14).

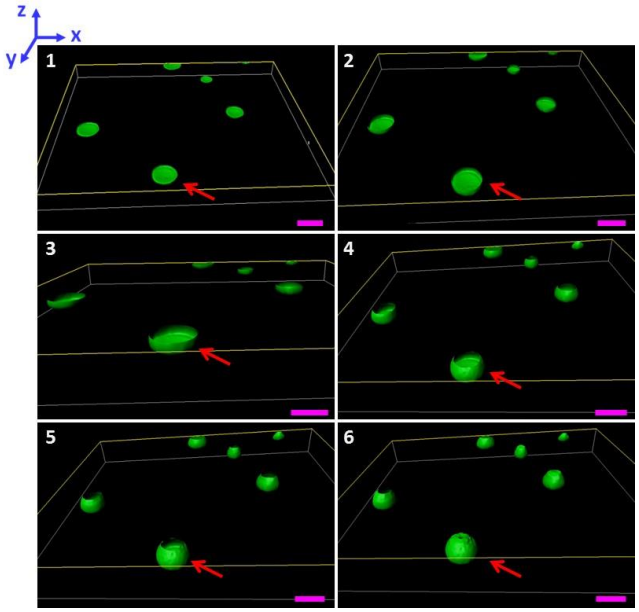

Figure 4. Reconstructed video frames for showing a 3D animation of hollow nanocapsules/vesicles produced after dissolution of **1** in acetone at a concentration above 7.9 mM. The sample was analysed in liquid state (acetone) by fluorescence confocal microscopy revealing their empty interior and fluorescent walls. Arrows indicate the formation of a particular vesicle through successive plans in zeta axis. Scale bars are 5 μm.

Complementary, concentrated solutions of compound **1** (7.9 mM) prepared in acetone and MeOH were studied in detail by confocal microscopy. To avoid instantaneous evaporation of the solvents during measurements and consequently changes in concentration of the sample, closed specimen holders were employed. The fluorescence imaging was performed on a Leica TCS SP5 confocal fluorescence microscope, and the image analysis and 3D reconstruction was carried out using the Bitplane Imaris software. The results corresponding to methanol solution were dismissed because the difficulty to achieve good images and 3D reconstructions. Unlike, the images obtained for compound **1** in acetone showed enough quality to have a 3D image reconstruction with good definition. As observed (Figure 4 and video in Supporting Information), the resulting images revealed the formation of hollow nanocapsules/vesicles in solution with an intense fluorescent emission around 450 nm mostly from the walls. This detailed morphological images corroborated the formation of hollow nanocapsules/vesicles in

solution at the related concentration rather than during the drying process.

Supramolecular assembly in water

The emission spectra of compound **1** in water (see Supporting Information, Figure S15a) show no structured emission bands, characteristic of the monomeric form, even at the lowest studied concentrations (3.9 10^{-3} mM), while a band at 450 nm already appears in diluted solutions and increases along the investigated concentration range (up to 7.9 10^{-1} mM). The fluorescence quenching observed at 3.9 mM, was ascribed to the formation of large non-emitting aggregates. The loss of the monomeric form is also observed in the excitation spectrum, which depicts a broad, unstructured band between 310-390 nm even at concentrations as low as 3.9 10^{-3} mM (see Supporting Information, Figure S15b). This spectral feature was already reported for pyrene in water solutions (λ_{emi} = 460 nm)[25] and was associated to the formation of microcrystals, confirming that in water **1** yields microstructures even at very low concentrations. Moreover, UV-Vis spectra of the water solutions of **1** show a broadening of the absorption bands in the 300-350 nm region (see Supporting Information, Figure S15c). The broadening of the bands becomes more evident upon increasing the concentration until collapsing in one broad and unstructured band (310-375 nm) at 7.9 mM. SEM/HR-TEM micrographs reveal a close relationship between morphologies for different ranges of concentrations and the spectroscopic data already shown. In this way, up to 3.9 mM belt-like nanostructures with ≈40 nm width and ≈2 nm thickness twisted to form superhelical bundles (see Supporting Information, Figure S16). On the other hand, above 3.9 mM, when a drop of fluorescence is observed, more compact plate-like aggregates are observed

Solvent-tuned supramolecular assembly of 1

The results suggested a structuration completely dependent on the solvent polarity and concentration. Thus, we can tune the morphologies from belt-like morphology or plates (in water) to hollow nanocapsules/vesicles (in MeOH or acetone). In this scenario, we decided to carry out a study in which the compound **1** dissolved in pure MeOH at concentration as high as 7.9 mM, was exposed to increasing volumes of water. The different samples were dried on the aluminum tape and analyzed by SEM (see Supporting Information, Figure S17). A first observation indicated that the preformed hollow nanocapsules/vesicles lose their spherical morphology as more water is added. When the water amount was less than 7.5%, coexistence of the two types of structures (hollow nanocapsules/vesicles and belt-like) were obtained. Above this concentration unique structuration in fibers first and then sheets was predominant. These last results motivate us to expose the compound **1** to cycles MeOH-water under the optimal conditions of structuration to check the ability of **1** to structure as hollow nanocapsules/vesicles in MeOH in a reversible manner. As expected, the hollow nanocapsules/vesicles were repeatedly reformed (at least up to 10 cycles) in MeOH (as long as the concentration was maintained around 7.9 mM), even starting from the structured **1** in water (Figure 5).

FT-IR analysis after each cycle of the dry sample in KBr pellets revealed which were the functional groups that presented most changes after structuring/destructuring process (see Supporting Information, Figure S18). In this way all the vibrations related with the acyl hydrazone (υN-H, υC=O, δN-H, and υC=N) and catechol (υO-H and υC-O) moieties showed variations. For example, N-H stretching band from hydrazone group in water was sharp and centered at 3250 cm^{-1}, while in MeOH was broadened and shifted to lower wavenumber (3205 cm^{-1}). Something similar occurred with the stretching band from O-H which changes from 3530 cm^{-1} in H_2O to 3450 cm^{-1} in MeOH, although in this case both signals presented much less intensity. Moreover, the region of amide (C=O) stretching vibrational mode showed in water a single band in comparison with that observed in methanol. This is an unambiguous signature of the presence of a network of intermolecular water-assisted H-bonded amides in the system.[15c]

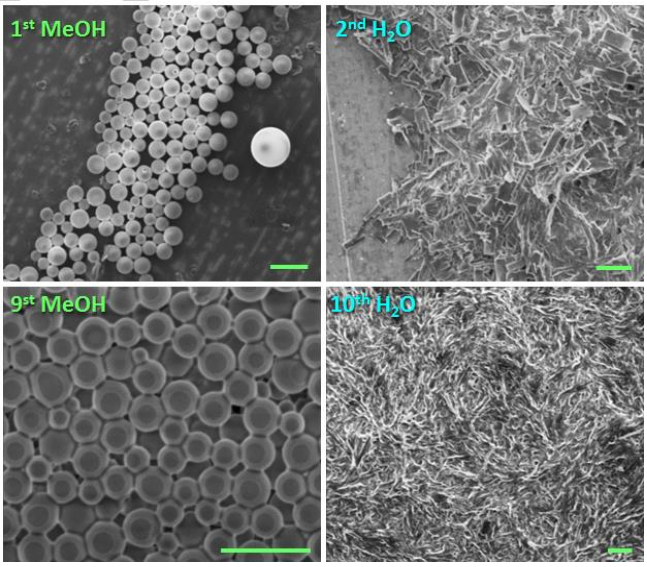

Figure 5. SEM images of compound **1** after MeOH-water cycles at 7.9 mM. Cycles 1 and 9 for MeOH and cycles 2 and 10 for water are shown revealing the successive formation of hollow nanocapsules/vesicles or belt-like structures depending of the solvent added. Scale bars are 2 μm.

Modeling of supramolecular interactions

In order to provide an atomistic interpretation of the obtained results, we have performed all atomic Molecular Dynamics (MD) simulations at ambient temperature and pressure of the compound **1** in two different solvents, MeOH and water. MD simulations are based on the numerical solution of the Newtonian equations of motion for all atoms the system under the given thermodynamic conditions. Obviously, a description with atomistic detail of the microsized particles observed experimentally is not possible nowadays. However, we can

study by simulations the ligand-solvent and ligand-ligand interactions which are responsible for the self-assembly processes behind the observed structures. Since experimental results in acetone and MeOH are very similar and all atomic MD simulations require a substantial computational effort, we have performed simulations only with MeOH and water as solvents.

We first consider simulations SIM1 (in MeOH) and SIM2 (in water) at ambient temperature and pressure of a single molecule **1**. In the Figure 6 we show a typical snapshot of the simulation results. For both solvents, simulations show the amphiphilic character of **1** since the solvophobic pyrene moiety does not present any significant interactions with the solvent molecules whereas the solvophilic catechol tail is observed to form hydrogen bonds with both solvents. We found four possible locations for solvent molecules interacting through hydrogen bonds with **1**, two at the –OH of the catechol groups and two at the hydrazide group. Being a dynamic system, not all four possible sites are occupied at the same time (Figure 6 is representative snapshot of the dynamic process). Our simulations give an average of 1.5 MeOH and 2.25 water molecules with hydrogen bonds with **1**. In both cases, half of the hydrogen bonds correspond to the catechol moieity and half to the amide. The pyrene moieity has unfavorable interactions with both solvents, and the formation of a clathrate cage around pyrene is seen in the simulations (not shown in the snapshots). This amphiphilic character (ability of tail to form hydrogen bonds and solvophobicity of the pyrene head group) is a driving force for self-assembly of **1** in both MeOH and water.

According to self-assembly thermodynamic theory,[26] the concentration at which self-assembly will occur and the structures formed depend both on the solvophobic/solvophilic balance in the **1** molecule and on the presence of attractive or repulsive interactions between **1** molecules. In order to identify the presence of interactions between compound **1**, we have considered atomistic MD simulations of two **1** molecules in a large solvation box, both for water and MeOH at ambient temperature and pressure (simulations SIM3 and SIM4 respectively, see technical details in Materials and Methods Section).

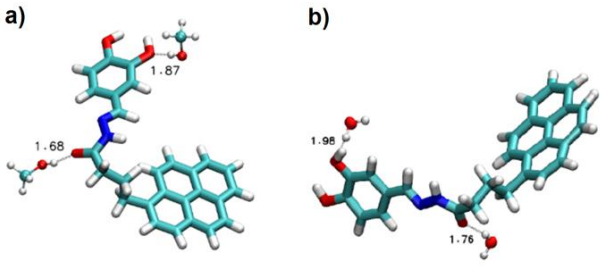

Figure 6. Snapshots from MD simulations corresponding to a single 1 molecule (licorice representation) in explicit solvent. For the sake of clarity we do not show all solvent molecules, we show only those solvent molecules that have hydrogen bonds with compound 1. These hydrogen bonded solvent molecules are shown in CPK representation and the hydrogen bond distances are given in Å.. (a) Simulation SIM1 with MeOH (b) Simulation SIM2 with water.

In this case, we obtain very different results for MeOH or water. In water (simulation SIM4), we observe a strong attractive interaction leading to preferred configurations with the pyrene groups in contact in face to face orientation (Figures 7a and 7b). The planes of the pyrene and catechol groups form an angle typically between 120º-130º. The catechol tails can be found in two different conformations: in close contact (see Figure 7a) or in opposite orientations (see Figure 7b). As the interaction between pyrene moieties determine the supramolecular assembly, the calculations of the pyrene-pyrene separation in the different possible conformations can give us information about the self-assembly process. Thus, while in water the histogram of pyrene-pyrene center of mass distances (simulation SIM4) has a sharp peak at about 6 Å, no significant

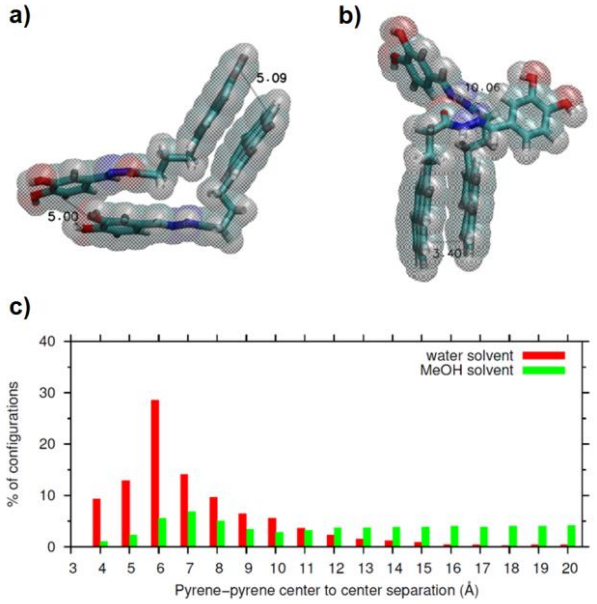

Figure 7. (a-b) Snapshots of simulation SIM4 corresponding to the interaction of two compound 1 molecules in water solvent. The representations show the molecules in their most probable configurations, with their pyrene groups in contact in face to face orientation. In (a) the catechol groups are also in close contact, whereas in (b) they are clearly separated (**1** molecules are shown in licorice representation and the Van der Waals size of the atoms is indicated as shadows). (c) Results from MD simulations SIM3 and SIM4, corresponding to the separation of pyrene moieties between two **1** molecules in different solvents. The histogram represents the **1**-**1** separation distances (measured between the centers of mass of pyrene groups) in MeOH solvent (SIM3 simulation) and water (SIM4 simulation).

1-**1** interactions (simulation SIM3) are observed in MeOH solvent (Figure 7c). From the simulation results, we can conclude that the self-assembly processes of **1** in MeOH and water are driven by different mechanisms. In the case of water, self-assembly is driven both by the amphiphilic character of **1** but also by the attractive interaction between pyrene groups (Figure 7). This attractive **1**-**1** interaction is responsible for the experimentally observed fact that even at very low concentrations, **1** molecules assemble in water. On the contrary, the self-assembly of **1** in MeOH is driven only by its amphiphilic character (Figure 7a), so it has a larger critical concentration C_c

for self-assembly. This critical concentration C_c is related to the gain in solvation free energy per molecule (chemical potential $\Delta\mu$) obtained from moving the solvophobic head of the molecule to a more favorable environment by the approximate relation $C_c \sim (1/v_s)\exp(-\Delta\mu/RT)$ (where R is the gas constant, T is the absolute temperature and v_s is the molar volume of the solvent). In our case, we can employ this equation to test the proposed driving force for self-assembly. In previous experiments,[27] it was estimated that the solvation free energy of pyrene in MeOH is about $\Delta\mu$=6.4 Kcal/mol = 11RT, so using a molar volume of 40.45 cm^3/mol for MeOH we predict for the critical concentration C_c ~ 4.0 10^{-1} mM. The calculated value is not far from the experimental concentration at which labile aggregates have been detected in MeOH (7.9 10^{-1} mM).

Based on what was experimentally/theoretically observed, we propose a tentative mechanism of the self-assembly behaviour in multidimensional structures (Figure 8). The molecules could form a dimer by π-π stacking and the hollow nanocapsules/vesicles could be composed of the cumulate dimmers induced by ethanol at high concentration. The intermolecular interactions, increase with the increase of molecules concentration and enhance the ability of molecular arrangement. By increasing the water % in solution the hollow nanocapsules/vesicles transform in thin helical fibres as stable conformation. The structures in pure water also can be tuned depending on concentration. Thus, at low concentration we keep the fiber-like structures, while if concentration is increased the material displays well-ordered 3D structures.

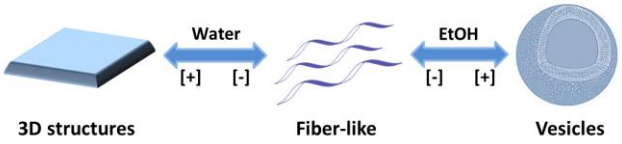

Figure 8. Schematic representation of the concentration and solvent-dependent self-assembly mechanism.

Conclusions

In summary, a very simple procedure for the formation of fluorescent hollow nanocapsules/vesicles in organic solvents has been reported. The amphiphilic molecule **1** containing hydrophobic pyrene and hydrophilic catechol groups is able to self-assemble in different solvents. While in water there is a strong interaction between pyrene moieties even at low concentrations which results in the formation of fibril-like aggregates (or microplates depending on the concentration), in MeOH the formation of supramolecular structures only occurs at higher concentration of **1**. Spectroscopic techniques confirmed that the self-assembly of **1** was related with vesicle formation in MeOH and acetone above 3.9 mM. Theoretical calculations led us to conclude that the self-assembly of compound **1** in water was driven by both the amphiphilic character (ability of catechol tail to form hydrogen bonds and solvophilicity of the pyrene head group) and the hydrophobicity and attractive interaction between pyrene groups. However, the self-assembly of **1** in MeOH was led by its amphiphilic character and dependent on the concentration. Interestingly, a reversible exchange of fibril-like nanostructures to vesicular ones could be achieved in successive addition cycles of MeOH or H_2O without losing the structures characteristic of both solvents indicating the reversibility of the self-assembly process.

Materials and Methods Section

Materials

All chemicals were purchased from Sigma–Aldrich and used without further purification. Solvents were purchased from Scharlab and used as received. Ultrapure water was generated using a Millipore Milli-Q system with a Milli-pak filter of 0.22 µm pore size and used for all the preparation of aqueous solutions.

Nuclear magnetic resonance (NMR) spectra were recorded on a Bruker ARX-400 and ARX-250 spectrophotometer using acetone-d_6. Fourier Transform Infrared Spectroscopy (FT-IR) spectra were collected on a Tensor 27 FT-IR Spectrometer (Bruker) in the range of 400-4000 cm^{-1} using KBr pellets. UV-Vis spectra were obtained on a Cary 4000 spectrophotometer (Agilent) using quartz cuvettes. Fluorescence emission was measured with a Hitachi F-2500 Fluorescence spectrophotometer with excitation and emission slits of 5 nm and a PMT voltage of 400 V. SEM images were obtained by a scanning electron microscope (FEI Quanta 650 FEG and FEI Magellan 400L XHR) at acceleration voltages of 2–5 kV. Aluminium tape was used as support. TEM images were obtained with a FEI Tecnai G2 F20 at a voltage of 200 kV, and a JEOL 1210 TEM operating voltage of 120 kV.

Optical and fluorescence images were registered by Zeiss Axio Observer Z-1 inverted optical/fluorescence microscope with motorized XY stage, Hg lamp excitation source, AxioCam HRc digital camera and standard filters. Fluorescence imaging was performed on a Leica TCS SP5 confocal fluorescence microscope. The image analysis and 3D reconstruction was performed using the Bitplane Imaris software.

Synthesis of compound 1

A mixture of 4-(pyren-1-yl)butanehydrazide (PBH, 0.06 mmol, 18 mg), 3,4-dihydroxybenzaldehyde (2, 0.05 mmol, 7 mg) and acetic acid (10 µL) in EtOH 96 % (6 mL) was stirred and heated under reflux for 6 hours. The solvent was then evaporated and the residue was washed with water and centrifuged. A pale yellow solid was obtained with a yield around 80%. Complete characterization is detailed in Supporting Information S1.

Simulation methods

We performed 4 different simulations, labeled here as S1, S2, S3 and S4. In simulations S1 and S2 we considered a single molecule of compound **1** in different solvents. In S1 we consider a box of 46.1 nm^3 containing 659 MeOH solvent molecules (4008 atoms in total) and in simulation S2, we consider a box of 57.4 nm^3 containing 1940 water molecules (5874 atoms). Simulations S3 and S4 correspond to simulations of two **1** molecules in different solvents and were prepared by adding another **1** molecule to simulations S1 and S2, respectively. All MD simulations reported here were performed using NAMD 2.11 software.[28] The molecular models were build using Visual Molecular Dynamics (VMD) and CGenFF software.[29,30] Inter- and intramolecular interactions between compound **1** and MeOH were described using the CHARMM

General Force Field.[30] For water molecules we employed the TIP4P/2005 force field,[31] which is the best model available in reproducing the hydrogen bonding features of liquid water.[32,33] Electrostatic interactions were computed using the PME method (PME) with the standard settings in NAMD (1 Å resolution, updated each 2 time steps). Lennard-Jones interactions were truncated at 1.2 nm employing a switching function starting at 1.0 nm. Temperature and pressure were kept constant at 298 K and 1 atm using a Langevin thermostat (relaxation time 1 ps) and the isotropic Nosé-Hoover-Langevin piston (oscillation period of 100 fs and decay time of 50 fs). Periodic boundary conditions were employed in all directions. The employed time step was 2 fs. Simulations S1 and S2 were ran for 10 ns. Simulations S3 and S4 required much longer runs (of 220 ns each) in order to obtain accurate statistics. All simulation snapshots were made with VMD. Data analysis was made using in-house build scripts running in VMD.

Acknowledgements

This work was supported by the project MAT2015-70615-R from the Spanish Government. K. W thanks Generalitat de Catalunya for her fellowship (Beca F1 2013). F. N. thanks Universidad Nacional del Sur for supporting her postdoctoral stay. DRM and JF acknowledge financial support from the Spanish Ministry of Economy and Competitiveness, through the "Severo Ochoa" Programme for Centres of Excellence in R&D (SEV-2013-0295 & SEV- 2015-0496). We thank CESGA Supercomputing centre for access to computational resources and technical support.

Keywords: catechol • self-assembly • vesicles • fluorescent • supramolecular

[1] J. Z. Zhang, Z.-l. Wang, J. Liu, S. Chen, G.-y. Liu in Self-assembled nanostructures, Eds.: D. J. Lockwood, Kluwer Academic Publishers, **2004**, pp. 7-13.

[2] P. Rajamalli, E. Prasad, *Langmuir* **2013**, 29, 1609−1617.

[3] R. Blumenthal, M. J. Clague, S. R. Durell, R. M. Epand, *Chem. Rev.* **2003**, *103*, 53–69.

[4] X. Zhang, Z. Chen, F. Würthner, *J. Am. Chem. Soc.* **2007**, *129*, 4886–4887.

[5] a) A. Ajayaghosh, C. Vijayakumar, V. K. Praveen, S. S. Babu, R. Varghese, *J. Am. Chem. Soc.* **2006**, *128*, 7174–7175; b) A. Ajayaghosh, V. K. Praveen, C. Vijayakumar, S. J. George, *Angew. Chem., Int. Ed.* **2007**, *46*, 6260–6265.

[6] a) A. L. Martin, B. Li, E. R. Gillies, *J. Am. Chem. Soc.* **2009**, *131*, 734–741; b) Y. Zhu, W. Tong, C. Gao, *Soft Matter* **2011**, *7*, 5805–5815; c) T. M. Allen, P. R. Cullis, *Science* **2004**, *303*, 1818–1822.

[7] a) J. Sedó, J. Saiz-Poseu, F. Busqué, D. Ruiz-Molina, *Adv. Mater.* **2013**, *25*, 653–701; b) J. Saiz-Poseu, J. Mancebo-Aracil, F. Nador, F. Busqué, D. Ruiz-Molina, *Angew. Chem., Int. Ed.* **2018**, https://doi.org/10.1002/ange.201801063.

[8] M. Guardingo, E. Bellido, R. Miralles-Llumà, J. Faraudo, J. Sedó, S. Tatay, A. Verdaguer, F. Busqué, D. Ruiz-Molina, *Small* **2014**, *10*, 1594–1602.

[9] J. Saiz-Poseu, J. Faraudo, A. Figueras, R. Alibes, F. Busqué, D. Ruiz-Molina, *Chem. Eur. J.* **2012**, *18*, 3056–3063.

[10] H. Ceylan, A. B. Tekinay, M. O. Guler, *Biomaterials* **2011**, *32*, 8797–8805.

[11] a) C. Yuan, J. Chen, S. Yu, Y. Chang, J. Mao, Y. Xu, W. Luo, B. Zeng, L. Dai, *Soft Matter* **2015**, *11*, 2243–2250; b) M. Krogsgaard, M. A. Behrens, J. S. Pedersen, H. Birkedal, *Biomacromolecules* **2013**, *14*, 297–301; c) N. Holten-Andersen, M. J. Harrington, H. Birkedal, B. P. Lee, P. B. Messersmith, K. Y. C. Lee, J. H. Waite, *PNAS*, **2011**, *108*, 2651–2655; d) Z. Shafiq, J. Cui, L. Pastor-Pérez, V. San Miguel, R. A. Gropeanu, C. Serrano, A. del Campo, *Angew. Chem. Int. Ed.* **2012**, *51*, 4332–4335; e) J. Guo, Y. Ping, H. Ejima, K. Alt, M. Meissner, J. J. Richardson, Y. Yan, K. Peter, D. von Elverfeldt, C. E. Hagemeyer, F. Caruso, *Angew. Chem., Int. Ed.* **2014**, *53*, 5546–5551.

[12] a) N.N. Adarsh, C. Frias, T.M. Ponnoth Lohidakshan, J. Lorenzo, F. Novio, J. Garcia-Pardo, D. Ruiz-Molina, *Chem. Eng. J.* **2018,** *340,* 94–102. b) M. Guardingo, P. González-Monje, F. Novio, E. Bellido, F. Busqué, G. Molnár, A. Bousseksou, D. Ruiz-Molina*, ACS Nano* **2016***, 10,* 3206−3213*;* c) M. Guardingo, F. Busqué, F. Novio, D. Ruiz-Molina, *Inorg. Chem.* **2015**, *54*, 6776−6781; d) M. Borges, S. Yu, A. Laromaine, A. Roig, S. Suarez-Garcia, J. Lorenzo, D. Ruiz-Molina, F. Novio, *RSC Adv*. **2015**, *5*, 86779–86783; e) F. Novio, J. Lorenzo, F. Nador, K. Wnuk, D. Ruiz-Molina, *Chem. Eur. J.* **2014**, *20*, 15443−15450; f) F. Novio, D. Ruiz-Molina, *RSC Adv.* **2014**, *4*, 15293–15296; g) I. Imaz, D. Maspoch, C. Rodriguez-Blanco, J. M. Perez-Falcon, J. Campo, D. Ruiz-Molina, *Angew. Chem., Int. Ed.* **2008**, *47*, 1857−1860; h) I. Imaz, J. Hernando, D. Ruiz-Molina, D. Maspoch, *Angew. Chem. Int. Ed.* **2009**, *48*, 2325 –2329; i) H. Ceylan, M. Urel, T. S. Erkal, A. B. Tekinay, A. Dana, M. O. Guler, *Adv. Funct. Mater.* **2013**, *23*, 2081–2090.

[13] a) M. Moriyama, S. Metzger, A. J. van der Vlies, H. Uyama, M. Ehrbar, U. Hasegawa, *Adv. Healthcare Mater.* **2015**, *4*, 569–575; b) U. Hasegawa, M. Moriyama, H. Uyama, A. J. van der Vlies, *Polymer* **2015**, *66*, 1–7.

[14] L. Bednarova, J. Brandel, A. du Moulinet d´Hardemare, J. Bednar, G. Serratrice, J.-L. Pierre, *Chem. Eur. J.*, **2008**, *14*, 3680–3686.

[15] a) J. Xu, L. Tao, C. Boyer, A. B. Lowe, T. P. Davis, *Macromolecules* **2011**, *44*, 299–312; b) N, Kameta, M. Masuda, T. Shimizu, *Chem. Commun.*, **2015**, *51*, 11104–11107; c) M, O. Guler, R. C. Claussen, S. I. Stupp, *J. Mater. Chem.*, **2005**, *15*, 4507–4512.

[16] R. Garifullin, M. O. Guler, *Chem. Commun.* **2015**, *51*, 12470–12473.

[17] F. M. Winnik, *Chem. Rev.* **1993**, *93*, 587–614.

[18] A. Salonen, A. Knyazev, N. von Bandel, J. Degrouard, D. Langevin, W. Drenckhan, *ChemPhysChem* **2011**, *12*, 150–160.

[19] a) H. T. Oyama, W. T. Tang, C. W. Frank, *Macromolecules* **1987**, *20*, 474–480; b) K. Char, C. W. Frank, A. P. Gast, W. T. Tang, *Macromolecules* **1987**, 20, 1833–1838.

[20] G. Bains, A. B. Patel, V. Narayanaswami. *Molecules* **2011**, *16*, 7909-7935

[21] J. F. Sinski, J. Exner, *Applied Spectroscopy*, **2007**, *9*, 970–977; b) B. C. MacDonald, S. J. Lvinb, H. Pattersonc, *Analytica Chimica Acta*, **1997**, *338*, 155–162.

[22] a) K. Kalyanasundaram, J. K. Thomas*, J. Am. Chem. Soc.*, **1977**, *99*, 2039–2044; b) D. C. Dong, M. A. Winnik, *Can. J. Chem.*, **1984**, *62*, 2560–2565.

[23] a) B. Jing, X. Chen, Y. Zhao, X. Wang, F. Ma, X. Yue, *J. Mater. Chem.* **2009**,*19*, 2037-2042; b) M. Changez, N.-G. Kang, C. H. Lee, J.-S. Lee, *Small* **2010**, *6*, 63–68.

[24] P. Rajamalli, E. Prasad, *Soft Matter* **2012**, *8*, 8896–8903.

[25] A. Nakajima, *J. Lumin.* **1977**, *15*, 277—282.

[26] S. A. Safran, *Statistical Thermodynamics of surfaces, Interfaces and membranes*, Addison-Wesley, **1994**, *Chapter 8*, 233-257 .

[27] D.B. Smithrud, F. Diederich, *J. Am. Chem. Soc.* **1990**, *112*, 339-343.

[28] J. C. Phillips, R. Braun, W. Wang, J. Gumbart, E. Tajkhorshid, E. Villa, C. Chipot, R. D. Skeel, L. Kale, K. Schulten, *J. Comput. Chem.* **2005**, *26*, 1781–1802.

[29] W. Humphrey, A. Dalke, K. Schulten, *J. Mol. Graphics Modell.* **1996**, *14*, 33–38.

[30] K. Vanommeslaeghe, E. Hatcher, C. Acharya, S. Kundu, S. Zhong, J. Shim, E. Darian, O. Guvench, P. Lopes, I. Vorobyov, A. D. MacKerell Jr., *J. Comput. Chem.* **2010**, *31*, 671–690.

[31] J. L. F. Abascal, C. Vega, *J. Chem. Phys.* **2005**, *123*, 234505–12.

[32] C. Vega, J. L. F. Abascal, *Phys. Chem. Chem. Phys.* **2011**, *13*, 19663–19688.

[33] C. Calero, J. Martí, E. Guàrdia, *J. Phys. Chem. B* **2015**, *119*, 1966–1973.

10.1002/chem.201802249

WILEY-VCH

FULL PAPER

Fluorescent catechol-based hollow nanocapsules/vesicles are obtained through a simple procedure that involves the dissolution in organic solvents of a simple amphiphilic molecule **1** containing a pyrene head and catechol tail. A correlation between the interaction of pyrene moieties giving supramolecular structures and vesicle formation according to concentration could be stablished through spectroscopic techniques as well as electron and confocal microscopies. Dispersion of compound **1** in water showed the formation of fibrillar structures assigned to ground state aggregates. Finally, reversible formation of hollow nanocapsules/vesicles or fibril-like nanostructures was obtained through successive cycles MeOH-H_2O at high concentrations.

F. Nador, K. Wnuk, C. Roscini, R. Solorzano, J. Faraudo, D. Ruiz-Molina, F. Novio**

Page No. – Page No.

Solvent-tuned supramolecular assembly of fluorescent catechol/pyrene amphiphilic molecules.